Preparation, analysis, and application of coated glass targets for the Wendelstein 7-X laser blow-off system

Th. Wegner,[1, a)] B. Geiger,[1, b)] R. Foest,[2] A. J. van Vuuren,[3] V. R. Winters,[1, 4] C. Biedermann,[1] R. Burhenn,[1] B. Buttenschön,[1] G. Cseh,[5] I. Joda,[4] G. Kocsis,[5] F. Kunkel,[1] A. Quade,[2] J. Schäfer,[2] O. Schmitz,[4] T. Szepesi,[5] and The W7-X Team[1, c)]

[1)] *Max-Planck Institute for Plasma Physics, 17491 Greifswald, Germany*
[2)] *Leibniz Institut für Plasmaforschung und Technologie e.V., 17489 Greifswald, Germany*
[3)] *Max-Planck Institute for Plasma Physics, 85748 Garching, Germany*
[4)] *University of Wisconsin-Madison, Madison, WI 53706, USA*
[5)] *Wigner Research Center for Physics, 1121 Budapest, Hungary*

Coated glass targets are a key component for the Wendelstein 7-X laser blow-off system that is used for impurity transport studies. The preparation and analysis of those glass targets as well as their performance is examined in this paper. The glass targets have a high laser damage threshold and are coated via physical vapor deposition with µm thick films. In addition, nm-thin layers of Ti are used as interface layer for improved ablation efficiency and reduced coating stress. Hence, the metallic or ceramic coating has a lateral homogeneity within 2% and contaminants less than 5% being optimal for laser ablation processing. With that method a short (few ms) and well defined pulse of impurities with about 10^{17} particles can be injected close to the last closed flux surface of Wendelstein 7-X. In particular, a significant amount of atoms with an velocity of about 1 km/s enters the plasma within 1 ms. The atoms are followed by a negligible concentration of slower clusters and macro-particles. This qualifies the use of the targets and applied laser settings for impurity transport studies with the laser blow-off system in Wendelstein 7-X.

Keywords: laser blow-off, laser ablation, thin film, coating, homogeneity, XPS, stellarator, impurity transport

I. INTRODUCTION

The removal of thin absorbing layers, e.g. metals, from transparent substrates like glasses by means of laser irradiation impact is called "laser ablation" or "laser blow-off" (LBO). This method can be divided into different cases depending on the side of irradiation, thicknesses of the layers and substrates as well as laser properties like pulse duration and wavelength[1]. These different ablation processes enable a wide-spread field of applications. In particular, the laser blow-off technique has been applied in fusion experiments for impurity transport studies[2–7], for electron heat transport investigation[8,9] and for plasma temperature and density measurement at the plasma edge[10–13]. It has also been used for studying atomic processes[14–18], patterning of thin film solar cells[19,20] as well as laser induced metal deposition[21].

The LBO system in the stellarator Wendelstein 7-X (W7-X)[22] is applied to inject non-intrinsic and non-recycling impurities to study their transport through the plasma[23–25]. The understanding of impurity transport is of utmost importance since impurities may lead, under specific conditions, to a degradation of the overall plasma performance or early pulse termination by increased radiative losses and dilution effects[26,27]. The experimental setup of the W7-X LBO system, as previously described by Wegner et al.[7], consists of a high energy laser, optical components and a glass target holder which is mounted on a manipulator to move the targets into the plasma vessel 600 mm away from the last closed flux surface (LCFS) being the boundary of the confined plasma region. The laser beam (Nd:YAG laser at 1064 nm with a pulse energy of 1 J and a pulse duration of 6 ns) is guided through movable lenses and mirrors to the glass targets. The glass targets are mounted with the coating facing towards the plasma side. The laser beam goes through the glass, hits the coating from behind and generates a small plasma on the glass surface[1]. This small plasma expands, blows-off and accelerates the ablated material, independently on the laser beam incident angle, perpendicular to the glass surface towards the plasma. Hence, the here considered LBO process can be classified as thin film glass side ablation. The application of LBO for impurity transport studies is advantageous since this method allows a repetitive and controlled injection of a well known amount of trace impurities with a defined spatial and temporal source function. However, the proper choice of laser settings and target materials has a very strong impact on the success of LBO experiments and requires detailed understanding of micro- and macro-scale properties. The optimization of the ablation process is proceeded via iterative ablation tests combined with the analysis of the ablated spots on the glass targets.

Hence, this paper describes the preparation of targets and the optimization of laser settings for the use of a glass side LBO for impurity transport studies in W7-X. Section II focuses on the applied coating methods while section III presents experimental results regarding the coating thickness and composition. The usage of the prepared glass targets for LBO impurity injection in W7-X is characterized in section IV of this paper. We can show, that these targets are highly suitable for that specific purpose which enables an important research field for fusion devices with the potential of steady state operation. Finally, a short summary is given.

[a)] Electronic mail: thomas.wegner@ipp.mpg.de, physics@thwegner.com
[b)] Present address: University of Wisconsin-Madison, WI 53706, USA
[c)] Author list in T. Klinger et al. Nucl. Fusion **59**, 112004 (2019)

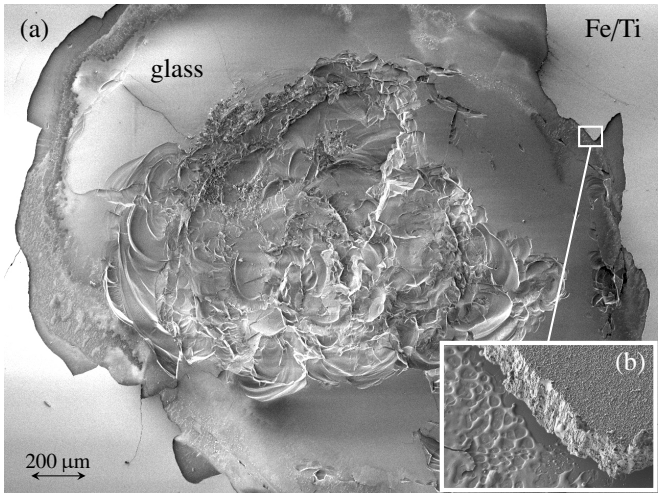

Figure 1. SEM micrograph of the ablation spot with a crater on the glass surface (a) and a zoom that visualizes the Fe/Ti coating in detail (b). The coating was blown-off with a laser energy density above the laser damage threshold at about 14 J/cm^2 creating a crater in the glass target. At the edge of the ablated spot where the laser energy is lower, a fraction of melted material stays on the glass surface albeit the coating is almost ablated (b).

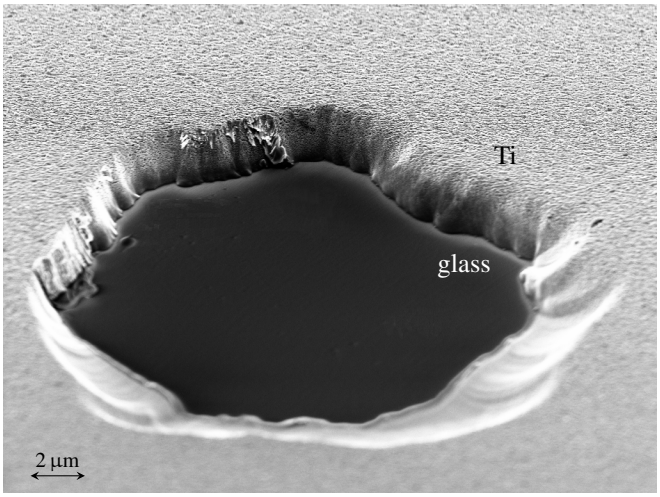

Figure 2. SEM micrograph of an ablated spot on a glass target which is coherently coated with Ti with a measured thickness of 2.0 ± 0.04 µm.

II. PREPARATION OF LBO TARGETS

The choice of appropriate glasses is a mandatory task for the high energy LBO of thin films. The different glass types can be classified according to their material, volume purity, surface quality and polish degree. Additionally, different key attributes like transmittance, homogeneity, inclusion and laser damage threshold result from the above mentioned classification. Hence, a suitable glass for a thin film glass side LBO has a high transmittance for the laser wavelength, a good homogeneity for a suitable and adherent coating and low inclusions to guarantee a high laser damage threshold. Here, fused silica glass targets (Corning® HPFS® 7980-5f, 45 × 45 × 2 mm^3) are chosen for LBO application and are coated via physical vapor deposition (PVD).

Thin coatings suitable for laser ablation are commonly deposited using PVD methods where the film material is provided from a solid target. Typical techniques are the direct current magnetron sputtering (MS) and electron beam evaporation (EB). The target material is sputtered by impinging ions (MS) or evaporated by an electron beam directed to a crucible which contains the target material (EB). Under low pressure conditions, the evaporated material is transported towards the substrate, where it condensates on the surface forming a thin coating (e.g. of ablation material as in this case) with typical growth rates of a few nm/s[28]. The process conditions have a major impact on the morphology, mechanical and optical properties of the resulting thin film. In the case of MS, the parameter governing the film properties is the amount of applied momentum and energy provided by the ions that are formed in the plasma and accelerated towards the target surface. In particular, the reduction of the bias voltage from 100 V to 60 V is a crucial optimization step to achieve homogeneous coatings with an adequate adhesion. Basically, the process condition for EB is chosen to ensure a uniform material evaporation, while maintaining a desirable high deposition rate of up to 4 nm/s and a preferably low temperature of the crucible. Additionally, a controlled substrate temperature can contribute to the reduction of inner stress. The deposition process itself heats up the substrate to temperatures of up to 450 K. Hence, the substrate is pre-conditioned thermally to 450 K prior to deposition to avoid accumulation of thermal stress.

For some materials, see the brackets in table I, a thin interface layer of Ti is additionally deposited on the glass prior to the actual coating used for ablation and injection. This slightly reduces the purity of the coating but improves the ablation performance since the applied laser radiation is absorbed significantly better on Ti than on Cu or Fe for example. Hence, this interface layer enables the ablation of the material with the applied laser energy density (see section III) with one shot. Without having a Ti interface layer for coating materials that have a high reflection coefficient for the used laser wavelength like Cu or Fe, a complete ablation with one shot is not possible even if the laser energy density is doubled. Additionally, the film adhesion on the glass surface can be significantly enhanced with a Ti interface layer. Moreover, it is observed, that the inner stress of the film can be alleviated by an intermediate layer that interrupts the columnar growth. Depending on the material and the coating thickness, this columnar growth can lead to an inhomogeneous coating with a broken surface. Hence, the deposition of a 5 µm thick film is suspended after the actual film has reached a thickness of 2.5 µm for the deposition of a 50 nm Ti interlayer. Afterwards, the deposition of the actual film is continued until the full thickness of 5 µm is reached.

To study the impurity transport and especially the impact of the nuclear charge[29], different materials are deposited with the above mentioned PVD methods on the glass targets. The materials listed in table I were injected into the plasma ves-

Table I. Overview of the coating and interface (in brackets) materials that were successfully applied for the W7-X LBO system together with the used PVD method (MS: magnetron sputtering, EB: electron beam evaporation) and the achieved coating thickness. Coating materials marked with ⋆ are analyzed in detail in this paper.

material (interface)	PVD method	thickness / µm
B_4C (Ti)	MS	6.2 (0.05)
Cu (Ti)	EB	2 (0.05)
Fe	MS	2
Fe (Ti)⋆	EB	5 (0.1)
Mo	MS	2
Mo (Ti)	EB	3.5 (0.05)
Ni	EB	2
Si	MS	5
Ti⋆	EB	2 & 5
W	MS	2.1

sel of W7-X during the operation phase OP1.2 owing to their well-studied emission characteristics. However, the following analysis and the characterization of the LBO injection focus only on Fe/Ti and Ti coated glass targets, without limiting the generality.

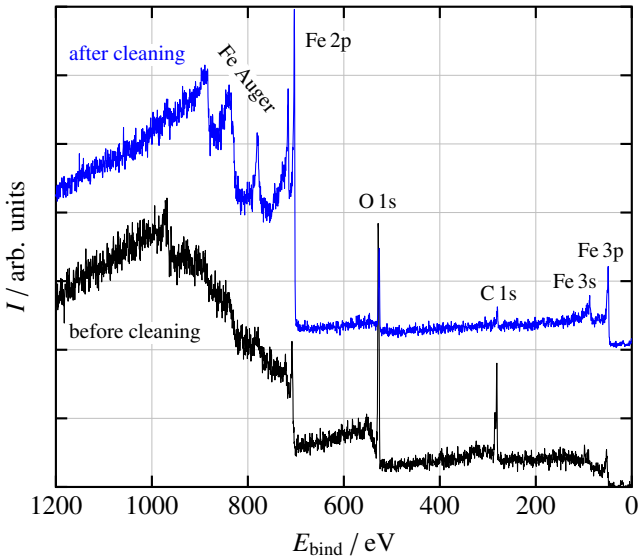

Figure 3. XPS overview spectra with the intensity over the binding energy before (bottom) and after (top) the cleaning of the surface via sputtering.

III. ANALYSIS OF THE COATED GLASS TARGETS

The analysis of the glass target and the coating is important to verify the applicability for LBO injections in a fusion device. Especially, the laser damage threshold of the glasses is a major property with respect to the application of high energy LBO. Hence, the glass targets which are used for the following experiments presented in this paper are analyzed with respect to their laser damage threshold. For that, the laser energy density on the target is varied to determine the threshold values by shooting once on the coated glass target from the glass side. Up to a laser energy density of $13\,J/cm^2$, the surface of the glass is not affected by the laser. A slight increase to $14\,J/cm^2$ leads to a well visible damage of the coating side surface only, see figure 1 (a). At a laser energy of $90\,J/cm^2$, the glass target gets cracks and the surfaces on both sides of the glass are damaged. However, the typical applied laser energy density at W7-X of $8\,J/cm^2$ (4 mm spot diameter at 1 J laser pulse energy) is low enough not to damage the glass but high enough to fully ablate the coating. Exemplarily, a full ablation of an Fe/Ti (thickness of 5 µm/0.1 µm) coating is observed for laser energy densities higher than $4\,J/cm^2$. Beside of other properties, this ablation threshold strongly depends on the reflectivity of the coating material[18]. This motivates the use of an interface layer as discussed in the previous section.

Beside of a high laser damage threshold, a coherent coating with high adhesion on the glass surface is essential for LBO applications. Hence, the homogeneity of the films is inspected after laser ablation using scanning electron microscopy (SEM). In figure 2 a SEM micrograph of an ablated spot is shown that illustrates a coherent and adherent coating. Using white light interferometry, the lateral profile from the glass surface (dark area in figure 2) to the remaining coating (gray area in figure 2) can be measured to determine the coating thickness assuming a complete ablation. Exemplarily, the thickness of an envisaged 2 µm Ti coating is measured as 2 ± 0.04 µm taken into account 17 ablation spots which are distributed over the whole glass target, see one ablation spot in figure 2. Hence, the coating methods which are described in section II produce a coherent coating with a sufficient lateral homogeneity within 2%.

To analyze the composition of the coatings, exemplary pure Fe films of 2 µm thickness are analyzed using X-ray photoelectron spectroscopy (XPS). The XPS spectra, see figure 3, are analyzed and charge corrected by shifting all peaks to the aliphatic C 1s spectral component set to a binding energy of 285 eV. To remove contaminants from the sample surface, it is sputtered in-situ with Ar^+ ions for 2 min. The XPS measurements are carried out before and after the cleaning. The elements O, C, and Fe are detected in the overview spectra, see figure 3. Since the information depth of XPS is typically 5 – 10 nm, only the outmost surface layer of the film is analyzed. Moreover, hydrogen, which is assumed to be also on the coating surface, cannot be detected by XPS. Before sputtering, the surface contains considerable amounts of C and O as well as N with an intensity close to the detection limit. These are surface contaminants and oxides acquired from the exposure to ambient air. The surface layers render the portion of Fe to only about 10%. After the sputtering process, the C peak decreases significantly, demonstrating the effective removal of the surface layer and the access of the analysis to the actual coating material. Traces of Ar with an intensity close to the detection limit are also detectable since it is contained in the gas mixture of the process and part of the Ar ions impinging on the surface are incorporated in the growing film. After the cleaning, the Fe 2p peak can be evaluated. According to the literature[30], the Fe $2p_{3/2}$ component can be exploited to

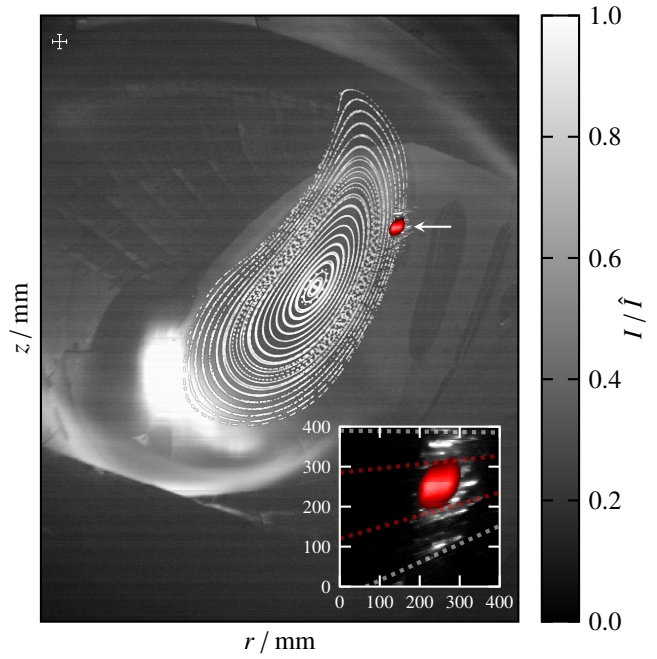

Figure 4. Cross section picture of the normalized emission intensity I measured in the visible spectral range inside the plasma vessel during the LBO injection (Fe) together with field lines for the standard magnetic field configuration in vacuum for the experimental program 20171012.022. The emission pattern from the injected particles is highlighted in red for the atoms and white for clusters and macro-particles. The inset shows a magnification of the emission pattern together with dotted lines indicating the opening angle. The cross in the upper left corner represents the positioning accuracy of the field lines.

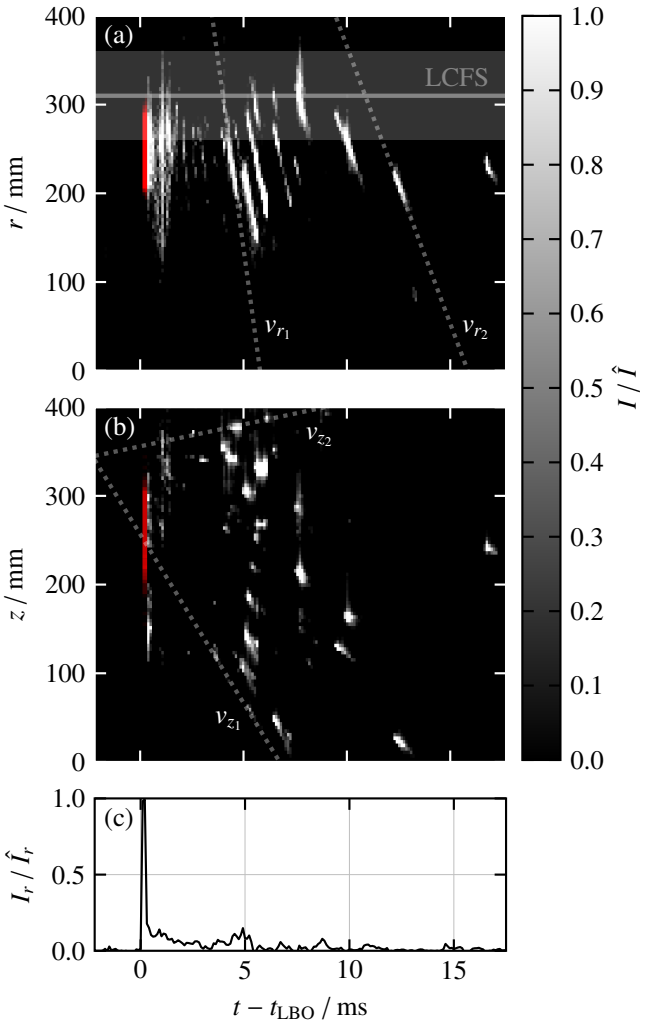

Figure 5. Normalized emission intensity I mainly of Fe I and II (atoms in red, clusters and macro-particles in white) integrated over the vertical (a) and horizontal (b) axis over the time and the time trace (c) of the radially integrated normalized emission intensity (a) for the experimental program 20171012.022. The dotted lines indicate the path of the injected clusters and macro-particles. The slope of those lines describes the individual velocity v of the particles. The radial position of the LCFS is indicated as solid line in (a) together with a shaded area indicating the positioning accuracy.

estimate the proportion of metallic Fe after performing a peak fitting procedure. Hence, the proportion of metallic Fe could be estimated to about 85% ± 1% whereas the proportion of Fe oxides is about 15% ± 1% showing a relatively pure coating with contaminants below 5%.

IV. CHARACTERIZATION OF LBO INJECTION FOR IMPURITY TRANSPORT STUDIES IN WENDELSTEIN 7-X

As mentioned before, the coated glass targets are used to inject impurities into the plasma of W7-X by means of LBO. The characterization of the impurity injection itself is important for further analysis, e.g., the implementation of transport codes that can describe the particle transport due to diffusion and convection.

For the analysis of the composition of the injected material, spectra taken by the high-efficiency extreme ultraviolet (XUV/VUV) overview spectrometer (HEXOS)[31] are used. Despite the surface contamination with C, O and N are measured by XPS, see section III, none of these impurities are found in the VUV spectra taken after an injection. Very weak Ti lines from the interface layer are possibly observed, but most of them are heavily superimposed by much stronger Fe lines and thus difficult to identify in the spectra due to the low concentration of about 2%. Hence, the contamination of the injected material is negligible and not taken into account for any further analysis based on LBO injection.

For modeling the impurity behavior in W7-X, it is important to know the amount and velocity of particles being injected into the plasma as atoms, clusters and macro-particles. An optimal condition can be achieved for LBO impurity injection at high atom to cluster/macro-particle ratios. This requires a high laser energy volume density[2,15,32,33], e.g., a high laser energy aimed on a thin coating. Additionally, the amount of clusters depends on the material[15]. The ablated amount of particles can be estimated after the ablation process taken

into account the measurement of the coating thickness, as described in section III, and the area of the ablated spot. Due to the sufficient lateral homogeneity that is shown in the previous section, the ablated volume and thus the amount of particles are inferred considering material specific quantities like the molar volume. In addition, one needs to consider the fraction of ionized particles generated by the ablation process since ions are deflected by the strong magnetic fields in W7-X and cannot reach the plasma. Hence, it is assumed that only 20% to 50% of the particles reach the LCFS[34]. This translates to about 10^{17} injected particles for a spot size of 4 mm^2.

Inside the plasma, the injected particles can be monitored in the visible spectral range with a video diagnostic system[35]. The event detection intelligent camera (EDICAM)[36] has the ability to simultaneously record visible radiation in independent regions of interest with different time resolution. When the injected particles reach the plasma, the neutrals as well as the lowest ionization stages start to emit in the deposition zone where the excitation becomes relevant. Thus, the location of the deposition zone as well as the dynamic behavior of the injected particles can be determined by measuring the emission in the visible spectral range, which, in the case of Fe, is mainly emitted from Fe I and Fe II. This is exemplarily visualized in figure 4 that shows a time-integrated cross section picture taken inside the plasma vessel during a discharge and an injection of Fe by means of LBO. Additionally, the cross section of the field lines for the standard magnetic field configuration in vacuum mapped in the poloidal plane of the LBO injection is shown. The injected Fe particles are visible as emission patterns (red for atoms, white for clusters and macro-particles), see also the inset in figure 4, in the deposition zone which is radially located at the LCFS. The temporal and spatial resolution ($\Delta z = \Delta r = 3$ mm, $\Delta t = 0.1$ ms) of the EDICAM is high enough to observe most of the clusters and macro-particles, individually. Hence, they can be easily distinguished from the fast and small atoms.

Since the poloidal plane of the LBO injection is almost perpendicular to the observation axis of the EDICAM, the angle as well as the velocity distribution of the injected particles can be estimated from the temporal evolution of the emission patterns shown in the inset of figure 4. An opening angle for atoms of about 15° is observed (red dotted line in the inset of figure 4), considering the spatial width of the radiating cloud and the distance between the LCFS, where the injected particles start to emit, and the surface of the glass target. The analysis of the angle distribution of clusters yields 30° (white dotted line in the inset of figure 4), possibly explained by the formation region in the edge of the ablation spot where the laser energy density is smaller compared to the center due to the laser beam profile. These angle distributions of the atoms and clusters are similar to the literature[2,15] and narrow enough to be a localized source of impurities in the W7-X plasma.

Thanks to the high time resolution of the EDICAM, the propagation speed of the radiating cloud of atoms, clusters and macro-particles can be analyzed. The velocity of the injected particles is mainly the result of the momentum transfer during the ablation process (mostly in horizontal direction) and is deflected by the gravitational force and drifts due to

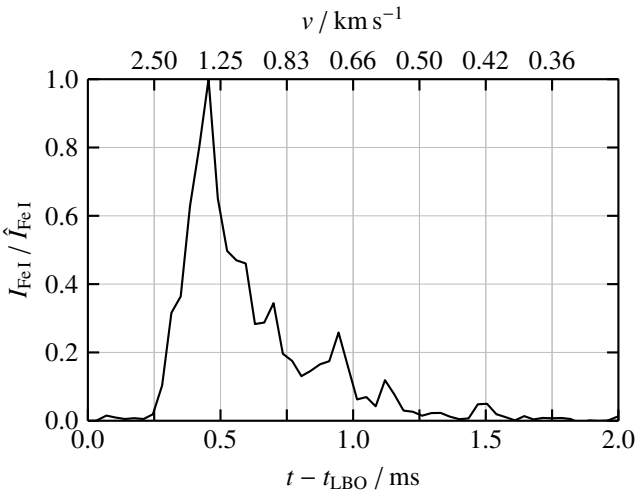

Figure 6. Normalized emission intensity of Fe I over the time after the laser pulse (bottom axis) and the velocity (top axis) of injected atoms for the experimental program 20180906.038. The velocity can be estimated within the uncertainty of ±5% due to the inaccuracy of the distance between the glass target surface and the deposition zone at the LCFS.

electric magnetic fields. The normalized emission intensity distribution of the particles (see the inset of figure 4), vertically (a) and horizontally (b) integrated, are shown in figure 5 for a time duration of 17.5 ms. The clearly visible peak at $t = 0$ can be attributed to the atoms which are faster due to the lower mass compared to clusters and macro-particles. Assuming that the emitting atoms move radially from one side of the observed emission pattern to the other side (from $r_1 = 300$ mm to $r_2 = 200$ mm) within 0.1 ms yields in zero order to an averaged velocity of about 1 km/s as lower limit. This is comparable with the literature[16,32,37,38] for the used laser energy density in the range of 2 – 30 J/cm^2. After the bright pattern of atoms, a lower intensity can be assigned to slower clusters that can be tracked individually. The velocity of the clusters can be determined from the slope of the dotted lines (distance over time) in figure 5 representing the path of the emitting particles. The assumption of a constant velocity is well reflected by the measurement of the emission, especially for the radial movement. As a result, the horizontal velocity of the fastest quantifiable cluster is about $v_{r_1} = 0.1$ km/s whereas the velocity for the slower clusters is about $v_{r_1} = 0.05$ km/s. The downward velocity is about $v_{z_1} = 0.05$ km/s and is one order of magnitude higher compared to the upward velocity v_{z_2} indicating the impact of additional forces. Hence, the kinetic energy of injected particles range between 0.05 . . . 30 eV for the here shown Fe injection.

The temporal behavior of the radially integrated emission intensity, see figure 5 (c), defines the source function and indicates that the particle cloud mainly consists of atoms since the intensity of the atomic beam is at least one order of magnitude higher compared to that of the clusters. In addition, the emission emitted from the ablated material reaching the plasma is measured by a high photon throughput Czerny-Turner like

spectrometer which uses aspherical quartz lenses for reduced transmission losses instead of mirrors. The emission at a central wavelength of 650 nm is focused onto a camera with an electron multiplying charge-coupled device (EM-CCD) chip which is operated in a burst mode setting that allows exposure times of 35 µs. The first burst is triggered by a pulse received directly from the laser system, such that the start of the burst is synchronized with the firing of the laser. Exemplarily, after 0.25 ms a sudden and sharp increase of the intensity is observed over the full spectrum indicating that the atoms reach the plasma and start to emit. Beside of a very intense Fe I line at 649.498 nm which is slightly overlapped with a weak O V line at 650.024 nm, several other lines associated with Fe I and II appear in the spectra. In figure 6, the temporal behavior of the Fe I lines (mainly from 649.498 nm) is shown over the time (bottom axis) after the laser pulse which was aimed on a Fe/Ti (thickness of 5 µm/0.1 µm) target. The velocity of the ablated atoms, see top axis in figure 6, reaching the plasma can be derived from the time difference between the received trigger and the first emission observation. For this simple estimation, it is assumed, that the particles move linear in time from the glass surface to the LCFS within a certain penetration depth without any retardation. Hence, uncertainties due to the distance estimation in the range of ±5% originate for the velocity determination of atoms for this specific ablation process. However, the velocity of the injected atoms is well in agreement with the literature[16,32,37,38] and the above mentioned rough estimation.

V. SUMMARY

Glass targets coated with Fe and Ti are exemplarily investigated with respect to their applicability for the impurity injection at W7-X. As a result, the glass targets and coatings have successfully been optimized for LBO studies leading to an overall success of the system. The coating of the fused silica glass targets by means of PVD methods produces thin films with a lateral homogeneity within 2% and a high purity with contaminants less than 5%. Additionally, these coated glass targets are qualified for this high laser energy LBO processing due to their high laser damage threshold. From a coating with a thickness of 5 µm about 10^{17} particles can be injected close to the LCFS of W7-X with a velocity between 0.05 km/s and 1 km/s. The distribution of injected particles, both in space and velocity, is perfectly suitable for impurity transport studies and can be used as experimental input data for transport analysis codes.

ACKNOWLEDGMENTS

The authors thank D. Köpp for technical assistance and performing the thin film deposition.
This work has been carried out within the framework of the EUROfusion Consortium and has received funding from the Euratom research and training programme 2014-2018 and 2019-2020 under grant agreement No 633053 and is partially funded by the U.S. Department of Energy under grant DE-SC00014210. The views and opinions expressed herein do not necessarily reflect those of the European Commission.

DATA AVAILABILITY

The data that support the findings of this study are available from the corresponding author upon reasonable request.

REFERENCES

[1] M. Domke, S. Rapp, M. Schmidt, and H. P. Huber, Applied Physics A **109**, 409 (2012).
[2] E. S. Marmar, J. L. Cecchi, and S. A. Cohen, Review of Scientific Instruments **46**, 1149 (1975).
[3] S. A. Cohen, J. L. Cecchi, and E. S. Marmar, Phys. Rev. Lett. **35**, 1507 (1975).
[4] R. Isler, Nuclear Fusion **24**, 1599 (1984).
[5] R. Burhenn, Y. Feng, K. Ida, H. Maassberg, K. McCarthy, D. Kalinina, M. Kobayashi, S. Morita, Y. Nakamura, H. Nozato, S. Okamura, S. Sudo, C. Suzuki, N. Tamura, A. Weller, M. Yoshinuma, and B. Zurro, Nuclear Fusion **49**, 065005 (2009).
[6] B. Zurro, E. Hollmann, A. Baciero, M. Ochando, F. Medina, K. McCarthy, E. Blanco, E. de la Cal, D. Carralero, M. Pedrosa, and TJ-II Team, Nuclear Fusion **51**, 063015 (2011).
[7] Th. Wegner, B. Geiger, F. Kunkel, R. Burhenn, T. Schröder, C. Biedermann, B. Buttenschön, G. Cseh, P. Drews, O. Grulke, K. Hollfeld, C. Killer, G. Kocsis, T. Krings, A. Langenberg, O. Marchuk, U. Neuner, D. Nicolai, G. Offermanns, N. A. Pablant, K. Rahbarnia, G. Satheeswaran, J. Schilling, B. Schweer, T. Szepesi, H. Thomsen, and the W7-X Team, Review of Scientific Instruments **89**, 073505 (2018).
[8] M. Kissick, E. Fredrickson, J. Callen, C. Bush, Z. Chang, P. Efthimion, R. Hulse, D. Mansfield, H. Park, J. Schivell, S. Scott, E. Synakowski, G. Taylor, and M. Zarnstorff, Nuclear Fusion **34**, 349 (1994).
[9] F. Ryter, R. Neu, R. Dux, H.-U. Fahrbach, F. Leuterer, G. Pereverzev, J. Schweinzer, J. Stober, W. Suttrop, ASDEX Upgrade Team, F. D. Luca, A. Jacchia, and J. Kinsey, Nuclear Fusion **40**, 1917 (2000).
[10] K. McCormick, Review of Scientific Instruments **56**, 1063 (1985).
[11] J. S. Bakos, G. Burger, I. B. Földes, P. E. Giese, P. N. Ignácz, G. Petravich, J. Szigeti, and S. Zoletnik, Plasma Physics and Controlled Fusion **31**, 693 (1989).
[12] D. Michaud, G. G. Ross, E. Haddad, H. H. Mai, A. Pospieszczyk, and J. P. St-Germain, Review of Scientific Instruments **63**, 5698 (1992).
[13] S. Sasaki, S. Takamura, Y. Uesugi, Y. Ohkouchi, and K. Kadota, Review of Scientific Instruments **64**, 2277 (1993).
[14] J. F. Friichtenicht, Review of Scientific Instruments **45**, 51 (1974).
[15] D. Manos, D. Ruzic, R. Moore, and S. Cohen, Journal of Vacuum Science and Technology **20**, 1230 (1982).
[16] S. Mattoo, L. Wirtz, A. Pospieszczyk, and B. Schweer, Nuclear Instruments and Methods in Physics Research Section B: Beam Interactions with Materials and Atoms **124**, 579 (1997).
[17] G. Heise, M. Englmaier, C. Hellwig, T. Kuznicki, S. Sarrach, and H. P. Huber, Applied Physics A **102**, 173 (2011).
[18] M. Domke, L. Nobile, S. Rapp, S. Eiselen, J. Sotrop, H. P. Huber, and M. Schmidt, Physics Procedia **56**, 1007 (2014).
[19] F. H. Karg, Solar Energy Materials and Solar Cells **66**, 645 (2001).
[20] S. Zoppel, H. Huber, and G. Reider, Applied Physics A **89**, 161 (2007).
[21] J. Bohandy, B. F. Kim, and F. J. Adrian, Journal of Applied Physics **60**, 1538 (1986).
[22] T. Klinger, T. Andreeva, S. Bozhenkov, C. Brandt, R. Burhenn, B. Buttenschön, G. Fuchert, B. Geiger, O. Grulke, H. Laqua, N. Pablant, K. Rahbarnia, T. Stange, A. von Stechow, N. Tamura, H. Thomsen, Y. Turkin, Th. Wegner, and the W7-X Team, Nuclear Fusion **59**, 112004 (2019).
[23] A. Langenberg, N. A. Pablant, Th. Wegner, P. Traverso, O. Marchuk, T. Bräuer, B. Geiger, G. Fuchert, S. Bozhenkov, E. Pasch, O. Grulke,

F. Kunkel, C. Killer, D. Nicolai, G. Satheeswaran, K. P. Hollfeld, B. Schweer, T. Krings, P. Drews, G. Offermanns, A. Pavone, J. Svensson, J. A. Alonso, R. Burhenn, R. C. Wolf, and the W7-X Team, Review of Scientific Instruments **89**, 10G101 (2018).

[24] A. Langenberg, F. Warmer, G. Fuchert, O. Marchuk, A. Dinklage, Th Wegner, J. A. Alonso, S. Bozhenkov, K. J. Brunner, R. Burhenn, B. Buttenschön, P. Drews, B. Geiger, O. Grulke, M. Hirsch, U. Höfel, K. P. Hollfeld, C. Killer, J. Knauer, T. Krings, F. Kunkel, U. Neuner, G. Offermanns, N. A. Pablant, E. Pasch, K. Rahbarnia, G. Satheeswaran, J. Schilling, B. Schweer, H. Thomsen, P. Traverso, and R. C. W. and, Plasma Physics and Controlled Fusion **61**, 014030 (2018).

[25] B. Geiger, Th. Wegner, C. Beidler, R. Burhenn, B. Buttenschön, R. Dux, A. Langenberg, N. A. Pablant, T. Pütterich, Y. Turkin, T. Windisch, V. Winters, M. Beurskens, C. Biedermann, K. J. Brunner, G. Cseh, H. Damm, F. Effenberg, G. Fuchert, O. Grulke, J. Harris, C. Killer, J. Knauer, G. Kocsis, A. Krämer-Flecken, T. Kremeyer, M. Krychowiak, O. Marchuk, D. Nicolai, K. Rahbarnia, G. Satheeswaran, J. Schilling, O. Schmitz, T. Schröder, T. Szepesi, H. Thomsen, H. Trimiño Mora, P. Traverso, D. Zhang, and the W7-X Team, Nuclear Fusion **59**, 046009 (2019).

[26] K. Ida, R. J. Fonck, S. Sesnic, R. A. Hulse, and B. LeBlanc, Phys. Rev. Lett. **58**, 116 (1987).

[27] A. Dinklage, K. McCarthy, C. Suzuki, N. Tamura, Th. Wegner, H. Yamada, J. Baldzuhn, K. J. Brunner, B. Buttenschön, H. Damm, P. Drewelow, G. Fuchert, M. Hirsch, U. Hoefel, H. Kasahara, J. Knauer, D. Maier, J. Miyazawa, G. Motojima, T. Oishi, K. Rahbarnia, T. S. Pedersen, R. Sakamoto, R. Wolf, D. Zhang, and the W7-X Team, Nuclear Fusion **59**, 076010 (2019).

[28] J. H. Powell, C. F.; Oxley and J. M. Blocher Jr, *Vapor Deposition* (Wiley, 1967).

[29] A. Langenberg, Th. Wegner, N. A. Pablant, O. Marchuk, B. Geiger, N. Tamura, R. Bussiahn, M. Kubkowska, A. Mollén, P. Traverso, H. M. Smith, G. Fuchert, S. Bozhenkov, H. Damm, E. Pasch, K.-J. Brunner, J. Knauer, M. Beurskens, R. Burhenn, and R. C. Wolf, Physics of Plasmas **27**, 052510 (2020).

[30] A. P. Grosvenor, B. A. Kobe, M. C. Biesinger, and N. S. McIntyre, Surface and Interface Analysis **36**, 1564 (2004).

[31] W. Biel, G. Bertschinger, R. Burhenn, R. König, and E. Jourdain, Review of Scientific Instruments **75**, 3268 (2004).

[32] J. Bakos, I. Földes, P. Ignácz, G. Kocsis, J. Szigeti, and J. Kovács, Optics Communications **74**, 374 (1990).

[33] J. S. Bakos, I. B. Földes, P. N. Ignácz, and G. Kocsis, Journal of Applied Physics **69**, 1231 (1991).

[34] K. Assmussen, "Untersuchungen zum Verhalten von Wolfram in Tokamakplasmen," IPP report 10/2, Garching: Max-Planck-Institut für Plasmaphysik (1996).

[35] G. Kocsis, T. Baross, C. Biedermann, G. Bodnár, G. Cseh, T. Ilkei, R. König, M. Otte, T. Szabolics, T. Szepesi, and S. Zoletnik, Fusion Engineering and Design **96-97**, 808 (2015).

[36] S. Zoletnik, T. Szabolics, G. Kocsis, T. Szepesi, and D. Dunai, Fusion Engineering and Design **88**, 1405 (2013).

[37] T. Yamauchi, M. Nagami, and S. Sengoku, Japanese Journal of Applied Physics **19**, 1737 (1980).

[38] J. Szigeti, J. S. Bakos, G. Bürger, P. N. Ignácz, M. A. Kedves, and L. Matus, Plasma Sources Science and Technology **5**, 32 (1996).